JOURNAL OF GEOPHYSICAL RESEARCH: SPACE PHYSICS, VOL. 118, 2958–2969, doi:10.1002/jgra.50308, 2013

On the influence of open magnetic flux on substorm intensity: Ground- and space-based observations

L. B. N. Clausen,[1] S. E. Milan,[2] J. B. H. Baker,[3] J. M. Ruohoniemi,[3] K.-H. Glassmeier,[1] J. C. Coxon,[4] and B. J. Anderson[5]

Received 13 November 2012; revised 12 April 2013; accepted 29 April 2013; published 04 June 2013.

[1] Using the location of maximum region 1 current determined by the Active Magnetosphere and Planetary Electrodynamics Response Experiment as a proxy for the open/closed field line boundary, we monitor the evolution of the amount of open magnetic flux inside the magnetosphere during 772 substorms. We then divide all substorms into three classes, depending on the amount of open flux at expansion phase onset. Studying the temporal variations during the substorms of each class for a number of related geophysical parameters, we find that substorms occurring while the amount of open flux is large are generally more intense. By intense we mean that the auroral electrojet, region 1 current, auroral brightness, tail dipolarization and flow speed, ground magnetic signatures, Pi2 wave power, as well as the intensity and extent of the substorm current wedge (SCW) are all larger than during substorms that occur on a contracted polar cap. The SCW manifests itself as an intensification of the nightside R1 and R2 current system after onset. Our analysis shows that to dispose of large amounts of accumulated open magnetic flux, large substorms are triggered in the terrestrial magnetosphere.

Citation: Clausen, L. B. N., S. E. Milan, J. B. H. Baker, J. M. Ruohoniemi, K.-H. Glassmeier, J. C. Coxon, and B. J. Anderson (2013), On the influence of open magnetic flux on substorm intensity: ground- and space-based observations, *J. Geophys. Res. Space Physics*, *118*, 2958–2969, doi:10.1002/jgra.50308.

1. Introduction

[2] Substorms have been studied for the past 50 years [*Akasofu*, 1964], primarily, because they have been recognized as one of the major agents in the coupling of the magnetosphere and the ionosphere. Substorms are preceded by a growth phase during which previously closed magnetic flux is opened and added to the magnetospheric tail through dayside reconnection. At some point, the magnetospheric tail becomes unstable due to the continued accumulation of open magnetic flux and magnetic reconnection inside the tail is triggered. The initial phase of tail reconnection is called the expansion phase, and during this phase, the previously open magnetic flux is closed. The expansion phase is followed by the recovery phase during which the magnetosphere gradually returns to a quiescent state. The combination of growth phase, expansion phase, and recovery phase is what constitutes a substorm.

[3] From the above qualitative description, it is clear that the amount of open magnetic flux inside the magnetosphere is a crucial parameter in determining the magnetospheric state. Its dynamics are governed by dayside and nightside reconnection rates, which are generally not equal [*Siscoe and Huang*, 1985]. Whereas the cause for dayside reconnection is relatively well understood and can be predicted quite well by monitoring the interplanetary magnetic field (IMF) upstream of the magnetosphere, the trigger of nightside reconnection, i.e., the trigger of the substorm expansion phase onset, is still debated. *Boakes et al.* [2009] identified the open/closed field line boundary (OCB) in global auroral images made by the IMAGE spacecraft which allowed them to estimate the amount of open magnetic flux in the magnetosphere. By comparing the relative occurrence of certain open magnetic flux values at substorm expansion phase onset with the occurrence of those values at other times, they were able to estimate the probability of a substorm occurring once a certain amount of open magnetic flux had been reached. They found a linear increase in the probability of a substorm occurring with increasing values of open magnetic flux. Their results indicated that there exists no critical threshold value of open magnetic flux at which a substorm is triggered. Studying the temporal evolution of the magnetospheric open magnetic flux content allows one to estimate the net reconnection rate and might help understand the triggering process. Furthermore, as substorms close previously

[1]Institute for Geophysics and Extraterrestrial Physics, TU Braunschweig, Braunschweig, Germany.
[2]Department of Physics and Astronomy, University of Leicester, Leicester, UK.
[3]Bradley Department of Electrical and Computer Engineering, Virginia Tech, Blacksburg, Virginia, USA.
[4]Department of Physics and Astronomy, University of Leicester, Leicester, UK.
[5]The Johns Hopkins University, Applied Physics Laboratory, Laurel, Maryland, USA.

Corresponding author: L. B. N. Clausen, Institute for Geophysics and Extraterrestrial Physics, TU Braunschweig, Germany. (l.clausen@tu-bs.de)

2169-9380/13/10.1002/jgra.50308

open magnetic flux, it is germane to ask how the amount of open magnetic flux at expansion phase onset influences the intensity of the substorm. *Milan et al.* [2009] previously showed that the intensity of the auroral signatures of substorms are dependent on their onset latitude; in this study, we bring a much wider data set to bear on this question, including in situ magnetotail observations.

[4] One way of estimating the amount of open magnetic flux in the magnetosphere is by identifying the boundary between open and closed magnetic field lines in the polar ionosphere. Once the OCB is found, the vertical component of some magnetic field model can be integrated over the area enclosed by the OCB to yield the amount of open magnetic flux. Such an identification of the OCB has been implemented by looking at particle precipitation spectra of low-Earth orbit satellites [*Newell et al.*, 1996], global auroral emissions [*Milan et al.*, 2003], spectral width of high-frequency radar backscatter [*Rodger et al.*, 1995], or ground-based magnetometer data [*Kamide et al.*, 1981].

[5] *Shukhtina et al.* [2004] presented a method based on work by *Petrinec and Russell* [1996] to derive the amount of open magnetic flux in the magnetospheric tail by estimating the lobe magnetic field and the tail radius from measurements of satellites crossing the magnetotail. In *Shukhtina et al.* [2004], they show that the total lobe flux is significantly enhanced during substorm intervals, consistent with magnetic flux loading of the tail. More recently, *Shukhtina et al.* [2009] expanded their methodology to allow for the prediction of lobe magnetic flux values based on upstream solar wind conditions.

[6] Recently, *Clausen et al.* [2013] showed that the maximum of the region 1 current [*Iijima and Potemra*, 1976] extracted from data by the Active Magnetosphere and Planetary Electrodynamics Response Experiment (AMPERE) is located about 1° equatorward of the OCB specified by Defense Meteorological Satellite Program (DMSP) data. In this study, we use AMPERE data to determine the location of the OCB and determine the strength of the magnetosphere-ionosphere coupling currents.

[7] *Rostoker et al.* [1980] defined three essential ingredients to the substorm expansion phase: (1) the intense brightening of an auroral arc and its rapid poleward expansion; (2) perturbations in midlatitude ground magnetometer data caused by field-aligned currents (FACs); and (3) at least one burst of Pi2 wave activity. Spacecraft measurements of plasma processes in the magnetospheric tail during substorms showed that substorms are associated with high-speed flows in the magnetotail [e.g., *Angelopoulos et al.*, 1994] as well as a change in the tail magnetic field configuration from more stretched to more dipolar [e.g., *Hesse and Birn*, 1991]. The latter process is commonly called "dipolarization" and usually identified in the magnetic field normal to the cross tail current sheet (B_Z).

[8] In this paper, we study how the amount of open magnetic flux at expansion phase onset influences the temporal variations and the intensities of all of these substorm signatures for 772 expansion phase onsets identified in all-sky imager data between January 2010 and April 2010.

2. Observations

[9] In this paper, we study average substorm intensities as a function of the amount of open magnetic flux in the magnetosphere. As a proxy for the auroral oval size, we use the amount of open magnetic flux in the magnetospheric system at substorm onset $Rf(t = T_0)$, or Rf_0 in short, where T_0 is the onset time of the substorm expansion phase. We determine *Rf* at any given time using data from the Active Magnetosphere and Planetary Electrodynamics Response Experiment (AMPERE). AMPERE is a facility funded by the National Science Foundation that increased the time resolution of the magnetic perturbation data provided by the Iridium® satellites by a factor of 10 to 20 s/sample during normal mode and by a factor of 100 in high-rate sampling when the resolution is increased to 2 s/sample. Using the technique described in *Waters et al.* [2001], the magnetic perturbations measured at ~700 km altitude by about 70 satellites in six orbital planes can be used to calculate the global distribution of vertical current densities, which at magnetic latitudes above ~60° correspond to the Birkeland currents or field-aligned currents (FACs) commonly associated with the region 1 (R1) and region 2 (R2) current system [*Iijima and Potemra*, 1978; *Cowley*, 2000]. Using AMPERE, the global radial current density can be estimated every 2 min, although a true update of the data occurs every 10 min commensurate with the inter-satellite time spacing in each orbit plane. The data used here were provided with a latitudinal resolution of 1° and a longitudinal resolution of 1 h magnetic local time (MLT), i.e., the resolution is double that provided by the orbit plane spacing of the spacecraft. *Clausen et al.* [2013] have shown that the oval of maximum R1 current automatically extracted from the AMPERE data set [*Clausen et al.*, 2012] is statistically located about 1° equatorward of the open-closed field line boundary (OCB) determined by DMSP precipitation data. For this study, we integrate the vertical component of the International Geomagnetic Reference Field over the area enclosed by the R1 current oval shifted poleward by 1° to obtain an estimate of the amount of open magnetic flux in the magnetosphere *Rf*. The average of all *Rf* values determined for this study was 0.55 GWb.

[10] A list of 829 substorms identified using all-sky imager data is available for January 2010 through March 2010 on the website of the Thermal Emission Imaging System (THEMIS) mission and was used in this study to give T_0, i.e., the substorm expansion phase onset time. The substorm onset times are determined by visual inspection of the all-sky images. For 772 of these events, we are able to determine the amount of open magnetic flux Rf_0 at the time of auroral onset (T_0) using the method described above. The distribution of Rf_0 is shown in Figure 1a. We divide the distribution into three classes, such that each class contains roughly an equal amount of events, about 250 onsets. Class I is those substorms that occurred on a contracted auroral oval, i.e., when the amount of open magnetic flux was small at onset (Rf_0 less than 0.56 GWb). Note that most of these onsets occurred on ovals that were smaller than the average oval (0.55 GWb) of the entire data set. Substorms occurring on a medium-size auroral oval belong to class II, and class III encompasses all those substorms that occurred on an expanded auroral oval (Rf_0 greater than 0.65 GWb). Figure 1 shows the extent of each class and the colored shaded areas give the parts of the distribution belonging to each substorm class. We show the distribution of the onsets in magnetic latitude (Figure 1b) and magnetic local time (Figure 1c). As mentioned, the onsets were identified in all-sky imager data,

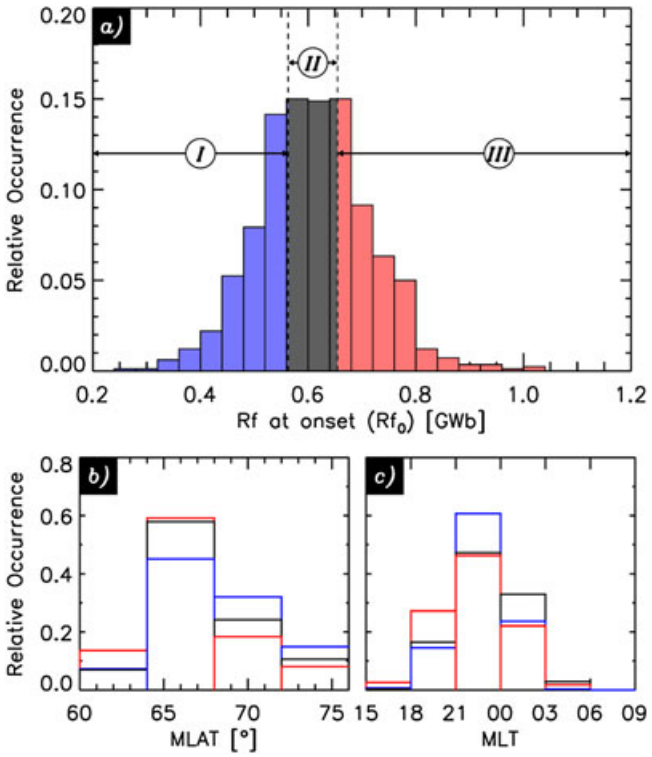

Figure 1. (a) Histogram of the open magnetic flux at substorm onset Rf_0. The distribution was divided into three classes I, II, and III with a roughly equal number of events, as indicated by the color shading and the markings. (a and b) Using the color scheme introduced in Figure 1a, the distribution of the substorm expansion phase onsets in magnetic latitude (Figure 1b) and magnetic local time (Figure 1c) is shown.

and we take the location of the center of the all-sky imager field-of-view at onset to produce Figures 1b and 1c. Both distributions are consistent with earlier, larger occurrence distributions were published by *Frey et al.* [2004]. Note also that, during onsets occurring while the amount of open magnetic flux in the magnetosphere is large (class III events), the onset latitude moves to lower values whereas the MLT distribution stays centered around 23 MLT.

[11] We then go on to perform superposed epoch analyses on important magnetospheric parameters centered on the time of substorm expansion phase onset. The analysis is done for the events in the three classes independently, such that for each parameter included in this study, we obtain three plots: each representing the average conditions during one of the substorm classes. As indicated in Figure 1, in our superposed epoch analysis, we use the color blue to represent class I behavior, black traces correspond to class II, and finally red lines are used to show the behavior during class III substorms. The analyzed parameters are shown in Figures 2–4, the median of the parameter distribution is shown as a thick line, upper and lower quartiles are shown as thinner lines. In both figures, the top panel shows the evolution of magnetic flux inside the R1 oval *Rf* for reference. As its value at T_0 is used to group the events, it is not surprising that class III substorms are associated with more open magnetic flux at onset. What is surprising, however, is that class I substorms are—on average—not closing any significant amount of flux according to our analysis. For this class of substorms, the amount of open magnetic flux is relatively constant throughout the 4 h interval centered around substorm onset. Only substorms of class II and III show a gradual increase prior to substorm onset and a gradual decrease following T_0. Two hours after T_0, the open flux content reaches levels around 0.55 GWb for all three substorm classes, indicating that class III substorms close significantly more magnetic flux after onset than class I and II substorms.

[12] The second row in Figure 2 shows the radius of the circle that was fit to the R1 current oval in the method of *Clausen et al.* [2012], i.e., the radius of the R1 oval *R1s* in degree. The dynamics of the open magnetic flux presented in the first row of Figure 2 is caused by the increase in *R1s* prior to substorm expansion phase onset, whereas the R1 oval contraction after T_0 causes a decrease in the amount of

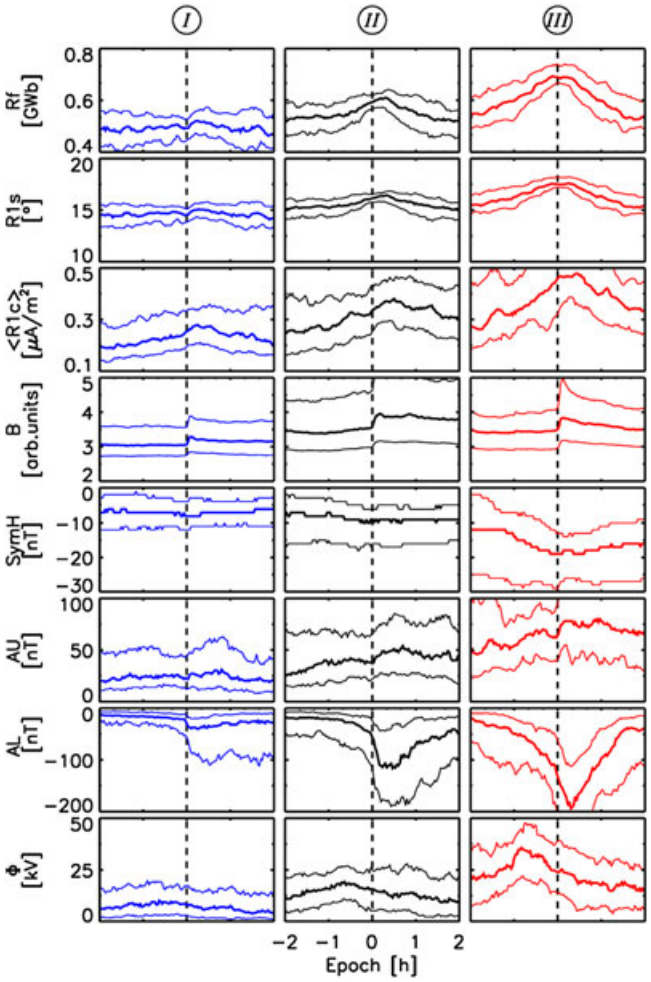

Figure 2. Superposed epoch analysis of various parameters for three classes of substorms as explained in the text. Medians during class I/II/III substorms are shown as thick blue/black/red lines, respectively. The upper and lower quartiles are shown as thinner traces. The parameters shown are the open magnetic flux, the median R1 oval radius, the median R1 current, the median auroral brightness, the SymH index, AU and AL indices, and the dayside reconnection rate.

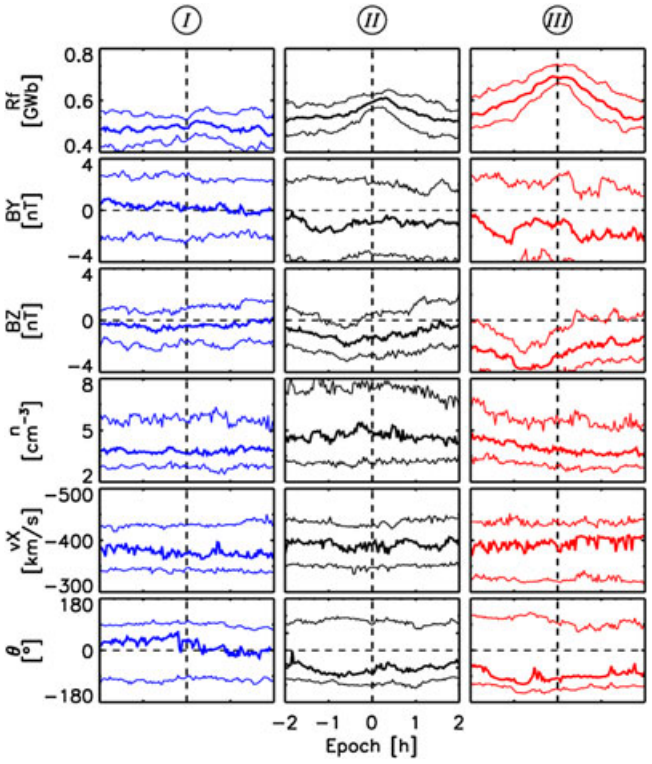

Figure 3. Superposed epoch analysis of various parameters for three classes of substorms as explained in the text. Medians during class I/II/III substorms are shown as thick blue/black/red lines, respectively. The upper and lower quartiles are shown as thinner traces. The parameters shown are the open magnetic flux, the IMF B_Y and B_Z components, the solar wind proton density, the solar wind velocity, and the IMF clock angle.

open magnetic flux. During the expansion phase of class III substorms, the amount of open magnetic flux decreases by about 0.13 GWB while the R1 oval shrinks by about 2.5°.

[13] The method by *Clausen et al.* [2012] allows one to extract the maximum R1 and R2 current density at all MLTs from AMPERE measurements. In the third row of panels in Figure 2, we show a superposed epoch analysis of the median of the R1 current over all MLTs. Grouping the substorms by Rf_0 nicely orders the amount of current flowing in the R1 system as well; the more the auroral oval is expanded at onset, the higher the current density both before and after T_0. Note that the maximum current is reached about 20 min after onset.

[14] All substorms studied here were identified using all-sky auroral imagers, and in the fourth row of panels of Figure 2, we show the evolution of auroral brightness for the three substorm classes. We calculate the brightness by integrating over the entire field-of-view of each imager at which the specific substorm was observed. Each brightness trace shows a distinct step of similar size at onset, however, the background brightness before onset is significantly lower for the class I and slightly lower for the class II events when compared to the class III events. About 20 min after onset, the brightness in class I events is still significantly smaller whereas class II and III events are virtually identical.

[15] In the following fifth, sixth, and seventh rows, we show the temporal behavior of geomagnetic indices; SymH is similar to Dst and is an indicator of the ring current intensity, AU and AL are used to characterized the eastward and westward electrojets, respectively. Again, sorting the substorms by the amount of open magnetic flux at onset orders the behavior of these indices: the larger the auroral oval at onset, the stronger the ring current at onset and the stronger the east- and westward electrojets during the growth and expansion phase of the substorm. The magnetic bay in the AL index, commonly associated with an enhanced westward electrojet due to the substorm current wedge, is significantly larger for class III events than for class I substorms. In the last row of Figure 2, we show the estimated rate of dayside reconnection Φ, following *Milan et al.* [2012] as

$$\Phi = \Lambda\, v_X^{4/3} \sqrt{B_Y^2 + B_Z^2}\, \sin^{9/2}\left(\frac{\theta}{2}\right) \quad (1)$$

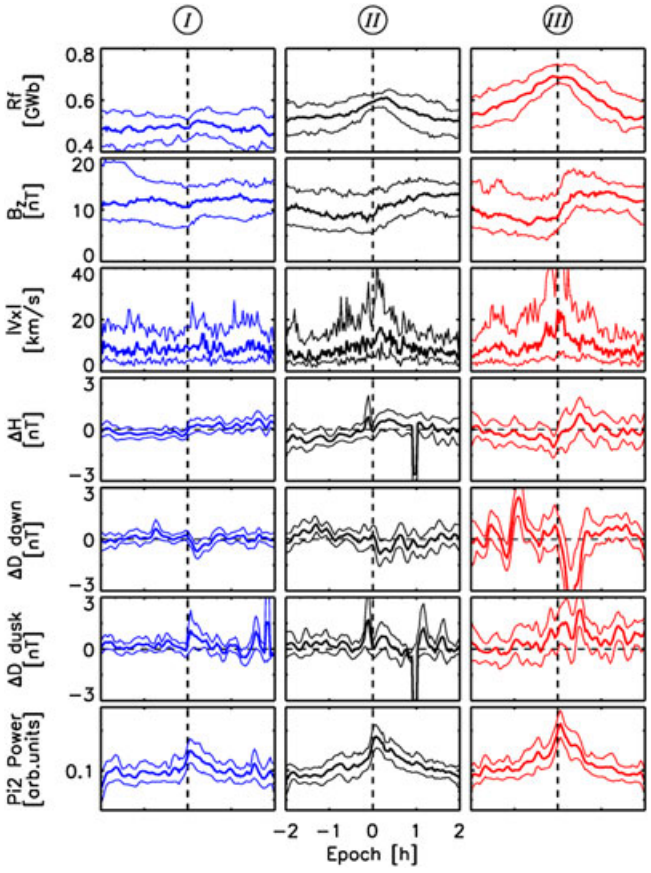

Figure 4. Superposed epoch analysis of various parameters for three classes of substorms as explained in the text. Medians during class I/II/III substorms are shown as thick blue/black/red lines, respectively. The upper and lower quartiles are shown as thinner traces. The parameters shown are the open magnetic flux, the magnetic B_Z component in the magnetospheric tail, the flow speed in X GSM direction in the magnetospheric tail, the midlatitude magnetic H (North-South) perturbation on the ground, the midlatitude magnetic D (East-West) perturbation on the ground in the pre-midnight sector followed by the magnetic D perturbation in the post-midnight sector, and the wave power in the Pi2 band observed at midlatitudes on the ground.

where v_X is the solar wind speed in the geocentric solar magnetospheric (GSM) X direction, B_Y and B_Z are the interplanetary magnetic field (IMF) components in the Y and Z GSM plane, and θ is the IMF clock angle, i.e., the angle between the IMF direction and the GSM Z direction. If B_Z is positive, we set Φ equal to zero. For the characteristic scale length Λ, we use 3.8 $R_e/(4 \times 10^5 ms^{-1})^{1/3}$ [*Milan et al.*, 2012]. As input for Φ, we use the OMNI solar wind data which is time shifted to the subsolar bow shock. Whereas for class I substorms, the dayside merging rate is nearly constant throughout the substorm interval; for class II and III, it shows significant increases prior to onset, indicating higher rates of dayside reconnection during the growth phase.

[16] As outlined in section 1, the solar wind conditions play a crucial role in the preconditioning of the magnetosphere prior to substorm expansion phase onset. In Figure 3, we show some important solar wind parameters for the three substorm classes. In the first row, we again show the evolution of the amount of open magnetic flux for reference. The following panels show the IMF B_Y and B_Z components, the solar wind proton density, the solar wind flow velocity in the GSM X direction, and the solar wind clock angle, i.e., the angle of the IMF direction in the GSM YZ plane. For substorms of class III, the IMF B_Y component is on average negative, the B_Z component shows a negative bay prior to substorm expansion phase onset. This is consistent with the increase in dayside coupling as expressed by the Φ parameter shown in the last row of Figure 2. The solar wind proton density and bulk flow velocity are relatively steady through the substorm phases. The same description qualitatively fits the observations during substorms of class II, however, the values of the IMF B_Z component prior to expansion phase onset are less negative than during the class III events. For class I, the IMF B_Z component is only slightly negative prior to the zero epoch. Furthermore, the auroral brightening observed on the ground seems associated, on average, with an IMF B_Y turning, as evident from the second and last panels. The bulk plasma parameters during class I events do not differ significantly from those during class II or III substorms.

[17] In Figure 4, we show more substorm related parameters. In the top row of Figure 4, we again show the average evolution of the open magnetic flux during our three classes of substorms for reference. In the next two panels, we show how the magnetospheric tail responded to the substorms studied. During those substorms where the THEMIS A satellite passed through the magnetospheric tail, we perform the same superposed epoch analysis in each of the three substorm classes as before. We only include satellite measurements obtained beyond a distance of –5 R_e downtail and within $\pm 5 R_e$ in the Y GSM direction. Even with these rather crude selection criteria for THEMIS data, Rf_0 orders the satellite measurements surprisingly well. The second row of panels displays the average magnetic B_Z component as measured by the flux-gate magnetometer on board the THEMIS A probe [*Auster et al.*, 2008]; the magnetic field was available during 617 of the 772 substorms studied here. The magnetic B_Z component is commonly associated with dipolarizations, i.e., with transitions of the magnetospheric tail from a stretched to a more dipolar field configuration. We can see from the second row of panels that, although the B_Z component is for all three classes around 10 nT 2 h before onset, just prior to onset B_Z is the smallest during class III events. The larger the open magnetic flux at onset, the more the magnetospheric tail is stretched prior to onset. The size of the dipolarization, i.e., the step in the B_Z component also increases with increasing auroral oval size at onset. Already 10 min past onset, the magnetic B_Z component is virtually the same for all three classes, recovering to slightly larger values 2 h after onset than it was at 2 h before. In the third row of panels, we show the bulk plasma speed in the X GSM direction; note that we show the average of the absolute flow speed, such that no conclusions about the direction of the flow can be made, i.e., whether the plasma was moving toward or away from Earth. These flow data were obtained by the ESA particle detector on board the THEMIS A probe [*McFadden et al.*, 2008], and data were available for 451 of the 772 substorms studied. The panels show that class III substorms are associated with the largest flow speeds just around onset. Note that, if we were to average the X direction flow speeds including their sign (not their absolute values as we have done here), the observed signature would disappear in the noise.

[18] In the fourth, fifth, and sixth rows of Figure 4, we show the magnetic perturbation in the H (North-South) and D (East-West) component observed at midlatitudes on the ground. At midlatitudes, i.e., relatively far away from the auroral electrojets, ground-based magnetometers observe magnetic perturbations due to the FACs associated with the substorm current system. This current system, the substorm current wedge (SCW), consists of a downward FAC on the eastern edge of the auroral electrojet and an upward FAC on its western edge [*McPherron et al.*, 1973]. The field-aligned parts of the SCW cause magnetic perturbations on the ground such that in the H component, a positive bay is observed at midlatitudes on the ground; at magnetometers located close to the upward part of the SCW, the D perturbation is positive, whereas near the downward FACs, the D perturbation is negative [*Clauer and McPherron*, 1974].

[19] The data shown in the fourth and fifth rows of Figure 4 were obtained by six magnetometer stations belonging to the THEMIS array located around 50° magnetic latitude in the American sector (see Table 1 for information about their locations). For each substorm event, we subtracted the mean value from the 4 h long time series of all three magnetic components and then performed the superposed epoch analysis. The resulting trace of the H perturbation in all three substorm classes shows a positive bay after substorm onset, however that bay associated with class III substorms is most pronounced. The same ordering appears when looking at the D (East-West) perturbation (see fifth and sixth rows). Here we have calculated the average evolution for the pre- and post-midnight sector independently in the same manner as described when discussing the H perturbation. It can be seen that after substorm onset all traces show a negative bay in the post-midnight sector and a positive bay in the pre-midnight sector. As the plots in both rows show, the larger the amount of open magnetic flux at substorm onset, the larger the magnetic perturbation observed on the ground at midlatitudes.

[20] Finally, in the last row of Figure 4, we show the wave power in the Pi2 band (periods between 40 s and 150 s, see *Jacobs et al.* [1964]). As mentioned earlier, Pi2 wave activity around expansion phase onset has been identified as

Table 1. Names, Abbreviations, and Locations in Geographic and Geomagnetic Coordinates of the Stations Used in the Analysis Presented in Figure 4

Name	Tag	Geog. Lat. [°]	Geog. Lon. [°]	Gmag. Lat. [°]	Gmag. Lat. [°]
Carson City	CCNV	39.19	240.22	45.35	304.84
Hot Springs	HOTS	47.59	245.34	54.31	307.96
Pine Ridge	PINE	43.11	257.40	51.39	323.14
Remus	RMUS	43.60	274.84	53.25	343.78
Loysburg	LOYS	40.17	281.62	50.08	352.21
Derby	DRBY	44.95	287.87	54.93	359.67

an integral part of the substorm process [*Baumjohann and Glassmeier*, 1984; *Keiling and Takahashi*, 2011]. For each magnetometer station listed in Table 1, we band-pass filter the data in the X (along magnetic North-South) and Y (along magnetic East-West) components between 6.6 mHz and 25 mHz. From each component time series, we calculate a moving FFT of length 1024 s and average the wave power over the two nearly field-perpendicular components. The Pi2 wave power is then the average Fourier power observed by all six magnetometer stations at midlatitudes in both the X and Y direction. Note that the y axis of those panels showing the Pi2 wave power is scaled logarithmically. Except for a small interval around substorm onset, the pulsation power is comparable for all three substorm classes. However, during this interval between about 10 min before and about 20 min after onset, the traces separate: class III substorms are associated with most Pi2 wave power, whereas during class I substorms, the Pi2 wave power is weakest.

[21] Our analysis of the ground-based magnetometer data shows that the larger Rf_0, the larger the magnetic perturbations both in the North-South and the East-West component (see fourth, fifth, and sixth rows in Figure 4). More pronounced magnetic bays indicate that the current flowing in the substorm current wedge (SCW) [*McPherron et al.*, 1973] was larger during the class III substorms than it was during the class I events [*Clauer and McPherron*, 1974]. Whereas the presented ground-based data are an indirect measure of the SCW intensity, AMPERE gives us the opportunity to study its strength more directly. In Figures 5–7, we show the average radial current density derived from AMPERE in the northern hemisphere on the nightside for the three classes of substorms, respectively. In each of the six panels of each figure, we show the currents at different times relative to the auroral onset, as given in the panel title. The median current densities were calculated for the three classes in a superposed epoch sense and are shown as non-filled blue and red contours in Figures 5,–7. Blue contours indicate currents flowing downward, i.e., into the polar ionosphere; red contours are used for the upward currents. The thick black trace in each panel shows the location of the R1 oval identified in the superposed current data using the methodology described in *Clausen et al.* [2013].

[22] Figure 5 shows that both R1 and R2 currents were—on average—well defined during the class I substorms. These currents were relatively stable in location and intensity throughout the period shown in Figure 5, which suggests that any activity in the FACs related to substorms is relatively weak when compared to the R1/R2 currents. To highlight changes in current density, we have calculated differences in current density on each grid cell between AMPERE current maps separated by 6 min and overlay these differences as filled contours. The filled contours are

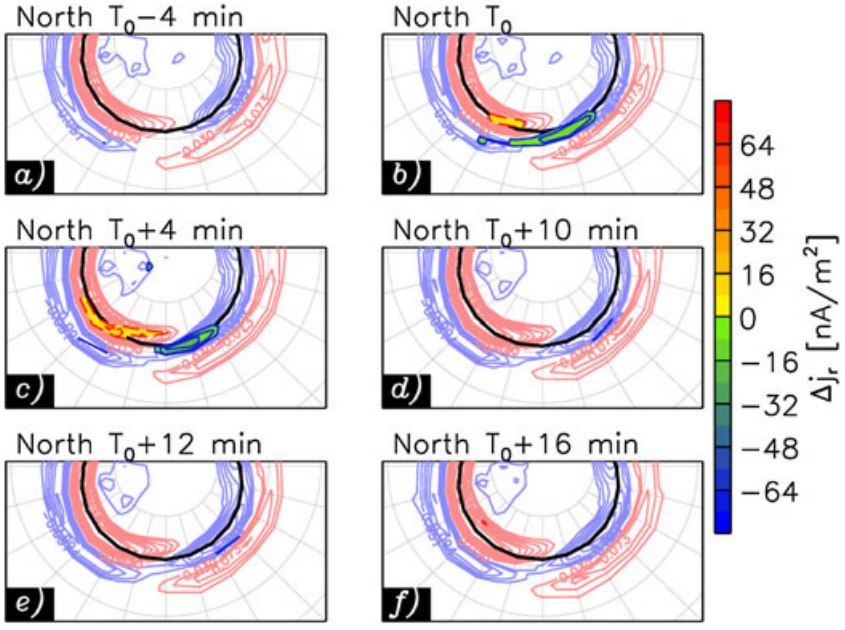

Figure 5. (a–f) View of the average radial currents in the northern hemisphere on the nightside during class I substorms (see text for details) at several times with respect to onset (T_0).

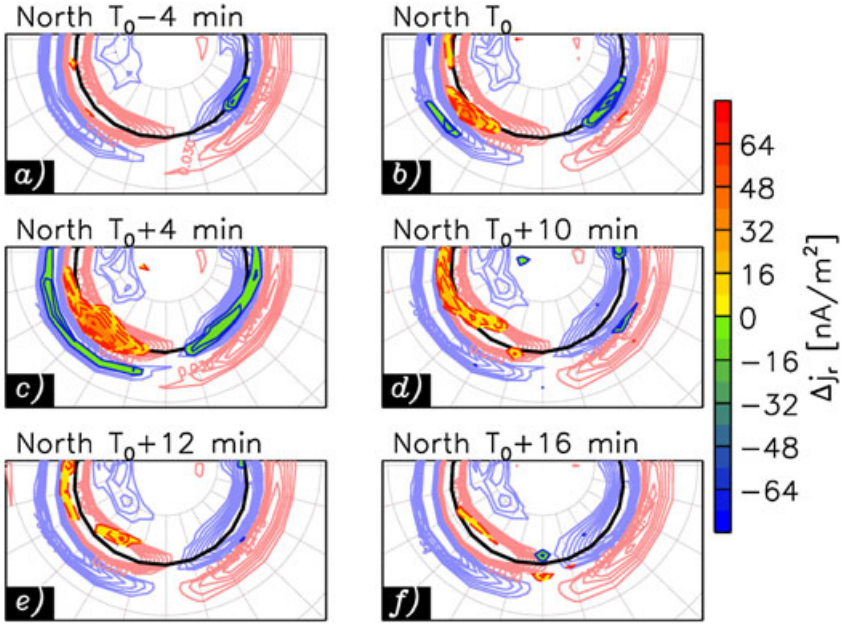

Figure 6. (a–f) View of the average radial currents in the northern hemisphere on the nightside during class II substorms (see text for details) at several times with respect to onset (T_0).

colored according to the color bar located right of the panels such that yellow-red contours denote increased upward current whereas green-blue contours indicate locations of increased downward currents.

[23] Our analysis shows that at expansion phase onset, the upward section of the nightside R1 current intensifies. This increased upward current is joined by a localized intensification of the downward section of the R1 current. The direction of these currents is consistent with the SCW. The center of the two current intensifications is shifted slightly toward the dusk sector, in agreement with the peak in onset MLT presented in Figure 1. We note that although no significant magnetic flux closure was observed during the class I events (compare second left panel in Figure 2), we do find evidence for the formation of the SCW and that it seems to be part of the R1 current system.

[24] In Figure 6, we show AMPERE current density data in the same format as Figure 5, however now for the class II substorms occurring on an average sized auroral oval. The R1 and R2 currents are stronger and located at lower

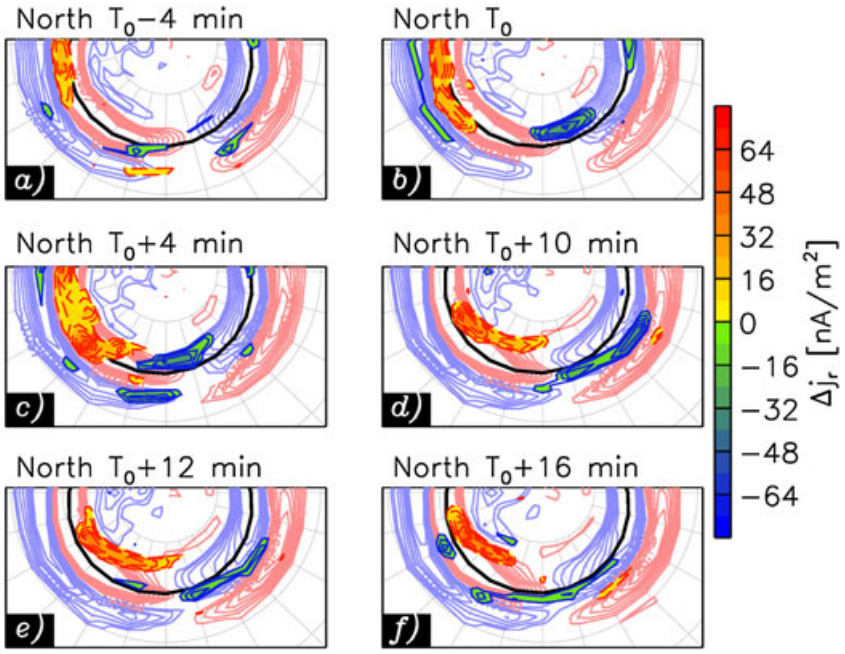

Figure 7. (a–f) View of the average radial currents in the northern hemisphere on the nightside during class III substorms (see text for details) at several times with respect to onset (T_0).

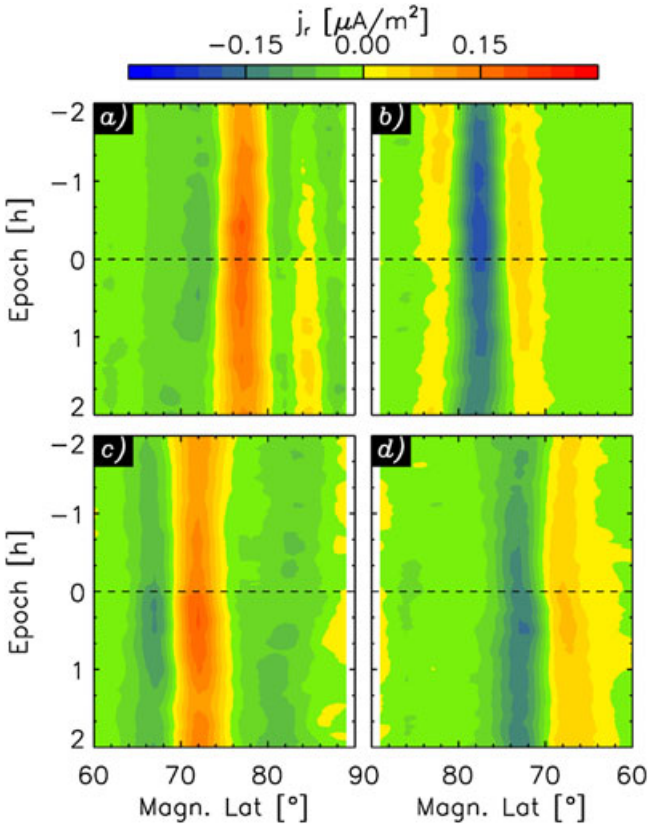

Figure 8. (a–d) The evolution with epoch time of the latitudinal variation of AMPERE current densities along four magnetic local times ("current keograms") is shown. Figures 8a–8d show the latitudinal current profile averaged between 14 to 16 MLT (dayside dusk), 08 to 10 MLT (dayside dawn), 20 to 22 MLT (nightside dusk), and 02 to 04 MLT (nightside dawn), respectively. In this figure, we show the currents resulting from the superposed epoch study for class I substorms in the northern hemisphere. The color bar gives the intensity of the currents with yellow to red colors representing current flowing out of the ionosphere, green to blue colors indicate current flowing into the ionosphere. The dashed horizontal line marks the substorm expansion phase onset.

latitudes when compared to the averages shown for class I events. When studying the current differences, we again find convincing evidence for the presence of the SCW. From the time of auroral onset until about 14 min after the current differences show a clear enhancement of the downward current (colored green) in the post-midnight sector at the R1 current location and a similarly intensified upward current located on the pre-midnight R1 current. The center of the transient current system is again shifted toward the dusk sector. Furthermore, the upward current of the SCW located in the dusk sector, which is associated with the auroral brightening, clearly moves poleward and slightly westward between onset and about T_0+10 min. This is consistent with auroral observations during substorms, showing the formation of a bright auroral bulge after onset that moves westward and poleward [*Akasofu*, 1964].

[25] Signature of the SCW becomes even more pronounced during class III substorms as shown in Figure 7. Although the magnitudes of the current changes do not increase significantly, the extent both in time and space of the SCW signature does. Again, the upward current of the SCW was moving poleward and slightly westward during the expansion phase, in agreement with the movement of the auroral bulge. At its most intense, AMPERE measurements suggest that the SCW carries about 0.3 MA which is a much smaller value than that inferred by *Clauer and McPherron* [1974], however, the magnetic perturbations on the ground (see Figure 4) are also much smaller and more importantly consistent with this estimate.

[26] In Figures 8–10, we show the evolution with epoch time of the superposed AMPERE current densities along four magnetic local times located in the dayside dusk, dayside dawn, nightside dusk, and nightside dawn sector for the three classes of substorms ("current keograms"). Figures 8a–10d display the temporal evolution of latitudinal current profiles averaged over 3 h MLT in each respective sector. Figures 8a–10d are arranged such that the location of each panel corresponds to the sector of which the data are shown when looking down onto a magnetic latitude/magnetic local time grid with the Sun toward the top, e.g., the latitude profiles of the dayside dawn sector are located in Figures 8b, 9b, and 10b.

[27] As in our previous plots of the current density distribution for class I substorms (Figure 5) in Figures 8a–d, the R1 and R2 currents are well defined between 2 h before and

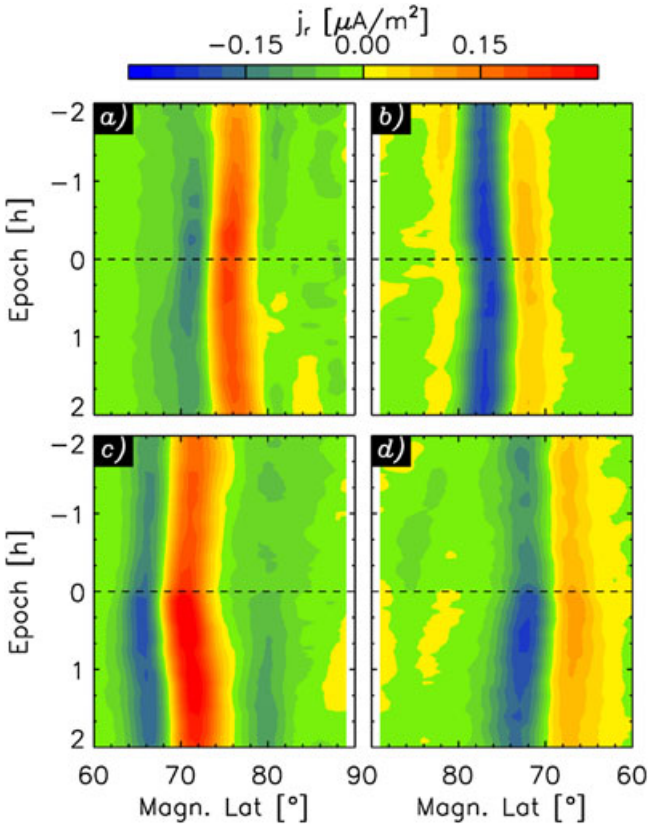

Figure 9. Current keograms around 15, 09, 21, and 03 MLT in the same format as Figure 8 but for class II substorms. The dashed horizontal line marks the substorm expansion phase onset.

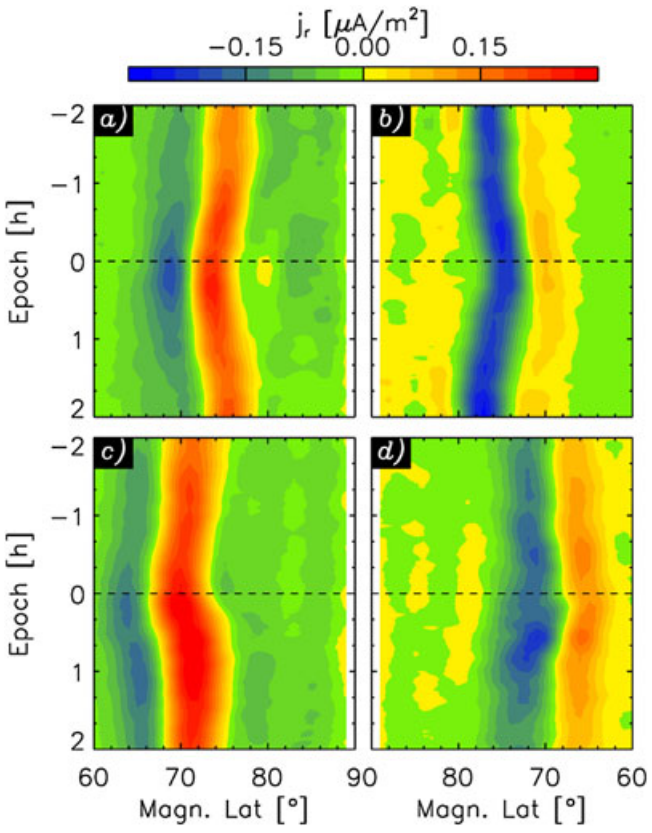

Figure 10. Current keograms around 15, 09, 21, and 03 MLT in the same format as Figure 8 but for class III substorms. The dashed horizontal line marks the substorm expansion phase onset.

after substorm onset. Figures 8a and 8c are from data measured at MLTs located in the dusk sector, such that the R2 current is directed into the ionosphere (colored green-blue) and the R1 current is directed outward (colored yellow-red). Accordingly, the poleward R1 current on the dawn flank (Figures 5b and 5d) is directed downward, whereas the R2 current is flowing out of the ionosphere. The data shown in Figures 8a and 8b are from the dayside and show an intensification of the R1 current prior to substorm onset, which is marked by a horizontal dashed black line. After onset, the dayside R1 current intensity decreases whereas an increase in nightside current density both on the dawn and dusk flank is observed (Figures 5c and 5d).

[28] During class II substorms (Figure 5), we do observe a latitudinal movement of the R1/R2 currents, particularly on the nightside (Figure 7c and 7d). The nightside current intensity peaks about 10–20 min after onset, consistent with the duration of the SCW shown in Figure 6. We note that the enhancement in dayside currents is observed during class II events also, however, it extends well into post-onset epoch times. The same observations apply to current keograms of substorms of class III (Figure 10). During these most intense events of our data set, the latitudinal movement of the currents is, in accordance with the significant accumulation and destruction of open magnetic flux, quite pronounced. Again the dayside currents dominate during the growth phase but are intensified until after expansion phase onset.

3. Discussion

[29] *Clausen et al.* [2012] have shown that the AMPERE data set provides the opportunity to estimate the location of the OCB by finding the ring of maximum region 1 current. From the OCB location estimate, we can compute the amount of open magnetic flux in the magnetosphere and then categorize substorms based on the amount of open magnetic flux at expansion phase onset. Furthermore, AMPERE gives us the opportunity to bin AMPERE current density measurements with respect to substorm expansion phase onset, i.e., compute global maps of FACs in a superposed epoch sense. The results presented in the previous section show that, on average, the amount of open magnetic flux present in the magnetosphere at substorm expansion phase onset determines the intensity of the substorm. The more open magnetic flux is stored inside the magnetosphere at onset, the stronger the substorm. By stronger, we mean that the auroral electrojet and the ring current are more enhanced, the dipolarization of the tail magnetic field is stronger, bulk plasma flows observed in the magnetospheric tail at onset are faster, and currents flowing in the R1/R2 current system as well as the substorm current wedge are stronger.

[30] An important aspect of the substorm process is the dipolarization of the magnetic field [*Hesse and Birn*, 1991], usually observed as a sudden increase of the magnetic B_Z component inside the magnetotail. Around the time of dipolarization, strong earthward and tailward flows are commonly observed [*Nakamura et al.*, 2001]. We find that the flow speeds and the dipolarization signature are strongest for substorms occurring on expanded ovals, consistent with our observations that more open magnetic flux is closed during these events. The observed increase in flow speed for substorms occurring on expanded ovals is also consistent with the increased amount of Pi2 wave power observed on the ground, as these flows are believed to drive Pi2 pulsations [e.g., *Frissell et al*., 2011].

[31] In Figures 5–7, we showed with the help of AMPERE data that the signature of the SCW is a localized current density enhancement colocated with the R1 current system, being an amplification of the same [*Barfield et al.*, 1986]. This intensification is stronger when the substorm occurs on an expanded auroral oval. Interestingly, whereas the SCW signatures in AMPERE data are very transient features that disappear within about 20 min of substorm onset, the depression in the AL index, which is a measure for the strength of the auroral electrojet that is thought to close the SCW in the polar ionosphere, lasts for much longer. As Figure 2 shows, AL only returns to at onset values about 1 h after onset for the class III events. Note that, in agreement with the short duration of the SCW in AMPERE data, the magnetic perturbations observed on the ground as well as the Pi2 wave power recover to pre-onset values within about half an hour after onset. The difference in duration between the SCW in AMPERE data and the recovery of the AL index might be explained by the fact that there exists significant current inside the R1 system even before and after expansion phase onset. The R1 current during the growth phase is mainly driven by increased dayside reconnection and must be closed by horizontal ionospheric currents which will create a signature in ground magnetograms. In fact, during events of all classes, the AL index begins to recover as the current flowing in the R1 system begins to decrease.

[32] Another apparent discrepancy is the delay between the maximum of the current in the R1 system and the maximum amount of open magnetic flux that can be seen in the first two rows of Figure 2. At expansion phase onset, the amount of open flux readily begins to decrease, whereas the R1 current maximizes about 20 min after onset. To investigate this offset, we produced plots of the R1/R2 current distributions in different local time sectors, particularly contrasting the current dynamics on the dayside (panels a and b in Figures 8–10) and on the nightside (panels c and d in Figures 8–10). In the expanding/contracting polar cap paradigm (ECPC) [*Lockwood and Cowley*, 1992; *Cowley and Lockwood*, 1992] dayside and nightside reconnection drive ionospheric convection which in turn is responsible for the generation of the R1 and R2 currents. This paradigm implies that dayside R1 currents are stronger during periods of dayside reconnection, whereas nightside reconnection drives FACs on the nightside. As shown in Figures 8–10, the nightside R1 and R2 currents intensify after substorm expansion phase onset, in agreement with the ECPC paradigm of nightside reconnection driving FACs there. This post-onset enhancement of the dayside currents together with the increasing nightside currents after onset is the cause for the continuous increase in R1 current even after onset. In summary, the continuing increase in overall R1 current past substorm expansion phase onset can be explained by the ongoing dayside merging even after onset while nightside reconnection intensifies nightside R1 currents. The sum of these two components produces the maximum of R1 current after substorm onset.

[33] In agreement with our observation that the amount of open magnetic flux inside the magnetosphere is hardly affected by class I events, no latitudinal movement of the R1 and R2 currents was observed (see Figure 8). However, because increased dayside and nightside currents were observed prior and after substorm expansion phase onset, which indicates increased dayside and nightside reconnection, we believe that these events are actual substorms and not pseudo-onsets. The fact that no change in the amount of open magnetic flux was detected by our method is indicative of the limits of accuracy of finding the amount of open magnetic flux using the R1 current oval as a proxy for the OCB. Note that all onsets of class I substorms occurred when the amount of open magnetic flux at onset was below the overall average flux value.

[34] Nightside dawn R1 currents were, during all three classes of substorms, about a factor of two smaller than their dusk counterpart, whereas the R2 currents in these two sectors are of comparable magnitudes. There was no such stark difference between the dayside currents. This nightside effect even persists if we choose the MLT range at which the current profiles are selected to reflect the shift of substorm onset MLT toward 23 h. *Anderson et al.* [2008] presented statistical distributions of FACs derived from Iridium magnetometer data as a function of upstream IMF conditions. Their results show that the IMF B_Y component influences the nightside R1 current intensity on both the dawn and dusk flank while the R2 current intensity is hardly affected. While the IMF B_Y positive conditions tend to decrease/increase the R1 currents on the nightside dusk/dawn flank, respectively, the R1 currents are weaker on the dawn side and stronger on the dusk side during IMF B_Y negative conditions. Since the substorms in our data set occurred during predominant IMF B_Y negative (compare second row of panels in Figure 3), weaker/stronger nightside dawn/dusk R1 currents are consistent with the statistical results presented in *Anderson et al.* [2008].

[35] We also note that, as Figures 5–7 show, there appears to exist no current continuity over the SCW, i.e., the upward current density in the west is larger than the downward current density in the east. This feature has been also reported by *Hoffman et al.* [1994] who use satellite magnetometer data to investigate the small scale features of FACs on the nightside during the substorm expansion phase. These observations are consistent with the fact that, in the region of the upward FACs, both the westward and eastward electrojets converge [*Kamide and Akasofu*, 1976]. The analysis by *Hoffman et al.* [1994] also show that the nightside FACs are composed of filamentary currents, a feature that cannot be resolved with the relatively coarse resolution of the AMPERE project.

[36] *Zaharia and Cheng* [2003] modeled the inner magnetospheric region during the substorm growth phase under the "slow-flow approximation," i.e., assuming that the temporal evolution of the magnetospheric state can be described as a series of snapshots, each of which depicting the system in force balance between the pressure gradient and Lorentz forces. Their results showed that by changing the magnetic field on their simulation boundary and the plasma pressure distribution in the equatorial plasma sheet, a realistic magnetospheric tail configuration as well defined R1/R2 currents on the nightside are produced. Furthermore, they showed that, compared with quiet time magnetic fields and plasma pressure distribution, during conditions that mimic the substorm growth phase, the R1/R2 currents on the nightside intensify and move to lower magnetic latitudes by about 4°. Although the simulation by *Zaharia and Cheng* [2003] did not include explicitly the effect of dayside reconnection, their results are consistent with our findings in the sense that adding open magnetic flux to the magnetospheric system will produce a more stretched magnetospheric tail which will in turn lead to a thinning of the plasma sheet and hence a change in the equatorial plasma pressure distribution. The current keograms presented in Figures 8–10 also show the intensification of the nightside R1/R2 currents prior to substorm expansion phase onset which, in view of the simulations by *Zaharia and Cheng* [2003], is due to changes in the gradients of the magnetic flux tube volume and the plasma pressure gradient [*Vasyliunas*, 1970].

[37] Numerical modeling of flow braking and low entropy bubbles propagating earthward has consistently shown that these features can form a current system compatible with the model of a SCW [*Birn et al.*, 1999; *Yang et al.*, 2012]. They also predict a secondary current loop, located equatorward of the SCW and with an opposite current sense, i.e., downward current in the dusk sector and upward current in the dawn sector. In Figure 6c, an increase in the downward R2 current on the dusk flank is observed 4 min after onset, in agreement with modeling results. We do not, however, observe an increased upward current in the dawn sector. In fact, the increase in current density seen in Figure 6c remains the only indication of the existence of a secondary current system associated with substorms using the data presentation shown in Figures 5–7. However, in the current

keograms of the nightside currents (Figures 8c and 8d, 9c and 9d, and 10c and 10d), clear enhancements of the R2 current after substorm expansion phase onset are observed. These enhancements last for roughly the same amount of time as the enhancements in the R1 current system, indicating that these are indeed signatures of the secondary R2 current system associated with earthward propagating low entropy bubbles predicted by numerical models.

[38] Our observations suggest that the SCW is formed after substorm expansion phase onset, centered on the MLT of the substorms auroral brightening, and that the SCW is an enhancement of the nightside R1 current system. At the same time, the R2 current system on the nightside also intensifies, consistent with numerical predictions of flow breaking. The enhancements in the R1 and R2 current systems are stronger for substorms that occur on expanded auroral ovals.

4. Summary

[39] *Clausen et al.* [2013] have shown that the R1 oval extracted from AMPERE data can be used as a meaningful proxy for the open/closed field line boundary such that one is able to estimate the amount of open magnetic flux in the magnetosphere around the time of substorm onset. We have investigated in a superposed epoch sense the temporal evolution of several magnetospheric parameters related to substorms. We divided a list of substorms into three classes: class I substorms occurred on a relatively contracted auroral oval, i.e., when the amount of open magnetic flux at onset was small. Class II substorms occurred when the auroral oval was of average size, and substorms belonging to class III appeared on an expanded auroral oval that enclosed a large amount of open magnetic flux. The more open magnetic flux is present at onset, the more current is flowing inside the R1 current system, the stronger the dayside merging electric field prior to onset, the stronger the auroral electrojet after onset, the greater the amount of current flowing inside the SCW, the larger the extent of the SCW, the more the tail magnetic field is dipolarized, the faster the flows observed in the magnetotail, and the stronger the Pi2 wave power observed on the ground. In conclusion, we find that the amount of open magnetic flux in the magnetosphere at expansion phase onset determines, on average, the intensity of the substorm. Studying the SymH index at substorm onset, we find that larger substorms tend to occur when the ring current is enhanced. Closer inspection of the distribution of the currents within the R1 system reveals that, in accordance with the expanding/contracting polar cap paradigm, dayside R1 currents dominate the growth phase, whereas nightside currents dominate the expansion phase. Due to continued dayside merging even after expansion phase onset, however, the dayside portion of the R1 current remains elevated even after substorm onset such that adding increased nightside currents due to initiated tail reconnection causes the overall R1 current to continuously increase. Only when the intensity of dayside merging decreases do the dayside R1 currents decay which, together with slowing reconnection in the tail as the substorm progresses, causes the overall R1 current to decrease about 20 min after expansion phase onset. The AMPERE current densities suggest that the SCW is an enhancement of the nightside R1 current system. At the same time, the R2 current system on the nightside also intensifies, consistent with numerical predictions of flow breaking.

[40] **Acknowledgments.** The authors would like to thank the THEMIS all-sky imager team for providing a list of substorm expansion phase onsets on their mission website at ftp://justice.ssl.berkeley.edu/events. LBNC acknowledges funding from the National Science Foundation under grant number ATM-0924919 and from the Deutsches Zentrum fuer Luft- und Raumfahrt under grant 50OC1102 and 50OC1001. SEM was supported by the Science and Technology Facilities Council (STFC), UK, grant ST/H002480/1. JCC was supported by an STFC studentship. The authors from Virginia Tech thank the National Science Foundation for support under grant AGS-0946900.

[41] Robert Lysak thanks the reviewers for their assistance in evaluating this paper.

References

Akasofu, S.-I. (1964), The development of the auroral substorm, *Planet. Space Sci.*, *12*, 273–+, doi:10.1016/0032-0633(64)90151-5.

Anderson, B. J., H. Korth, C. L. Waters, D. L. Green, and P. Stauning (2008), Statistical Birkeland current distributions from magnetic field observations by the Iridium® constellation, *Ann. Geophys.*, *26*, 671–687, doi:10.5194/angeo-26-671-2008.

Angelopoulos, V., et al. (1994), Statistical characteristics of bursty bulk flow events, *J. Geophys. Res.*, *99*, 21,257–+, doi:10.1029/94JA01263.

Auster, H. U., et al. (2008), The THEMIS fluxgate magnetometer, *Space Sci. Rev.*, *141*, 235–264, doi:10.1007/s11214-008-9365-9.

Barfield, J. N., N. A. Saflekos, R. E. Sheehan, R. L. Carovillano, and T. A. Potemra (1986), Three-dimensional observations of Birkeland currents, *J. Geophys. Res.*, *91*, 4393–4403, doi:10.1029/JA091iA04p04393.

Baumjohann, W., and K.-H. Glassmeier (1984), The transient response mechanism and Pi2 pulsations at substorm onset - Review and outlook, *Planet. Space Sci.*, *32*, 1361–1370, doi:10.1016/0032-0633(84)90079-5.

Birn, J., M. Hesse, G. Haerendel, W. Baumjohann, and K. Shiokawa (1999), Flow braking and the substorm current wedge, *J. Geophys. Res.*, *104*, 19,895–19,904, doi:10.1029/1999JA900173.

Boakes, P. D., S. E. Milan, G. A. Abel, M. P. Freeman, G. Chisham, and B. Hubert (2009), A statistical study of the open magnetic flux content of the magnetosphere at the time of substorm onset, *Geophys. Res. Lett.*, *36*, L04,105, doi:10.1029/2008GL037059.

Clauer, C. R., and R. L. McPherron (1974), Mapping the local time-universal time development of magnetospheric substorms using mid-latitude magnetic observations, *J. Geophys. Res.*, *79*, 2811, doi:10.1029/JA079i019p02811.

Clausen, L. B. N., J. B. H. Baker, J. M. Ruohoniemi, S. E. Milan, and B. J. Anderson (2012), Dynamics of the region 1 Birkeland current oval derived from the Active Magnetosphere and Planetary Electrodynamics Response Experiment (AMPERE), *J. Geophys. Res.*, *117*, A06233, doi:10.1029/2012JA017666.

Clausen, L. B. N., J. B. H. Baker, J. M. Ruohoniemi, S. E. Milan, S. Wing, S. Ohtani, and B. J. Anderson (2013), Temporal and spatial dynamics of the region 1 and 2 Birkeland currents during substorms, *J. Geophys. Res. Space Physics*, *118*, doi:10.1002/jgra.50288.

Cowley, S. W. H. (2000), *Magnetosphere-Ionosphere Interactions: A Tutorial Review*, pp. 91–106, Magnetospheric Current Systems, AGU, Washington, D. C., doi:10.1029/GM118.

Cowley, S. W. H., and M. Lockwood (1992), Excitation and decay of solar wind-driven flows in the magnetosphere-ionosphere system, *Ann. Geophys.*, *10*, 103–115.

Frey, H. U., S. B. Mende, V. Angelopoulos, and E. F. Donovan (2004), Substorm onset observations by IMAGE-FUV, *J. Geophys. Res.*, *109*, A10304, doi:10.1029/2004JA010607.

Frissell, N. A., et al. (2011), First radar observations in the vicinity of the plasmapause of pulsed ionospheric flows generated by bursty bulk flows, *Geophys. Res. Lett.*, *38*, L01,103, doi:10.1029/2010GL045857.

Hesse, M., and J. Birn (1991), On dipolarization and its relation to the substorm current wedge, *J. Geophys. Res.*, *96*, 19,417, doi:10.1029/91JA01953.

Hoffman, R. A., R. Fujii, and M. Sugiura (1994), Characteristics of the field-aligned current system in the nighttime sector during auroral substorms, *J. Geophys. Res.*, *99*, 21,303, doi:10.1029/94JA01659.

Iijima, T., and T. A. Potemra (1976), The amplitude distribution of field-aligned currents at northern high latitudes observed by Triad, *J. Geophys. Res.*, *81*, 2165–2174, doi:10.1029/JA081i013p02165.

Iijima, T., and T. A. Potemra (1978), Large-scale characteristics of field-aligned currents associated with substorms, *J. Geophys. Res.*, *83*, 599–615, doi:10.1029/JA083iA02p00599.

Jacobs, J. A., Y. Kato, S. Matsushita, and V. A. Troitskaya (1964), Classification of geomagnetic micropulsations, *J. Geophys. Res.*, *69*, 180–+, doi:10.1029/JZ069i001p00180.

Kamide, Y., and S.-I. Akasofu (1976), The auroral electrojet and field-aligned current, *Planet. Space Sci.*, *24*, 203–213, doi:10.1016/0032-0633(76)90017-9.

Kamide, Y., A. D. Richmond, and S. Matsushita (1981), Estimation of ionospheric electric fields, ionospheric currents, and field-aligned currents from ground magnetic records, *J. Geophys. Res.*, *86*, 801–813, doi:10.1029/JA086iA02p00801.

Keiling, A., and K. Takahashi (2011), Review of Pi2 models, *Space Sci. Rev.*, *161*, 63–148, doi:10.1007/s11214-011-9818-4.

Lockwood, M., and S. W. H. Cowley (1992), Ionospheric convection and the substorm cycle, in *Proceedings of the International Conference on Substorms (ICS-1)*, pp. 99–109, European Space Agency, Kiruna, Sweden, ESA SP-335.

McFadden, J. P., C. W. Carlson, D. Larson, J. Bonnell, F. Mozer, V. Angelopoulos, K.-H. Glassmeier, and U. Auster (2008), THEMIS ESA first science results and performance issues, *Space Sci. Rev.*, *141*, 477–508, doi:10.1007/s11214-008-9433-1.

McPherron, R. L., C. T. Russell, and M. P. Aubry (1973), Satellite studies of magnetospheric substorms on August 15, 1968. 9. Phenomenological model for substorms, *J. Geophys. Res.*, *78*, 3131–3149, doi:10.1029/JA078i016p03131.

Milan, S. E., M. Lester, S. W. H. Cowley, K. Oksavik, M. Brittnacher, R. A. Greenwald, G. Sofko, and J. Villain (2003), Variations in the polar cap area during two substorm cycles, *Ann. Geophys.*, *21*, 1121–1140, doi:10.5194/angeo-21-1121-2003.

Milan, S. E., A. Grocott, C. Forsyth, S. M. Imber, P. D. Boakes, and B. Hubert (2009), A superposed epoch analysis of auroral evolution during substorm growth, onset and recovery: Open magnetic flux control of substorm intensity, *Ann. Geophys.*, *27*, 659–668, doi:10.5194/angeo-27-659-2009.

Milan, S. E., J. S. Gosling, and B. Hubert (2012), Relationship between interplanetary parameters and the magnetopause reconnection rate quantified from observations of the expanding polar cap, *J. Geophys. Res.*, *117*, A03226, doi:10.1029/2011JA017082.

Nakamura, R., W. Baumjohann, R. Schödel, M. Brittnacher, V. A. Sergeev, M. Kubyshkina, T. Mukai, and K. Liou (2001), Earthward flow bursts, auroral streamers, and small expansions, *J. Geophys. Res.*, *106*, 10,791–10,802, doi:10.1029/2000JA000306.

Newell, P. T., Y. I. Feldstein, Y. I. Galperin, and C.-I. Meng (1996), Morphology of nightside precipitation, *J. Geophys. Res.*, *101*, 10,737–10,748, doi:10.1029/95JA03516.

Petrinec, S. M., and C. T. Russell (1996), Near-Earth magnetotail shape and size as determined from the magnetopause flaring angle, *J. Geophys. Res.*, *101*, 137–152, doi:10.1029/95JA02834.

Rodger, A. S., S. B. Mende, T. J. Rosenberg, and K. B. Baker (1995), Simultaneous optical and HF radar observations of the ionospheric cusp, *Geophys. Res. Lett.*, *22*, 2045–2048, doi:10.1029/95GL01797.

Rostoker, G., S.-I. Akasofu, J. Foster, R. A. Greenwald, A. T. Y. Lui, Y. Kamide, K. Kawasaki, R. L. McPherron, and C. T. Russell (1980), Magnetospheric substorms - Definition and signatures, *J. Geophys. Res.*, *85*, 1663–1668, doi:10.1029/JA085iA04p01663.

Shukhtina, M., N. Dmitrieva, and V. Sergeev (2004), Quantitative magnetotail characteristics fordifferent magnetospheric states, *Ann. Geophys.*, *22*, 1019–1032, doi:10.5194/angeo-22-1019-2004.

Shukhtina, M. A., E. I. Gordeev, and V. A. Sergeev (2009), Time-varying magnetotail magnetic flux calculation: A test of the method, *Ann. Geophys.*, *27*, 1583–1591, doi:10.5194/angeo-27-1583-2009.

Siscoe, G. L., and T. S. Huang (1985), Polar cap inflation and deflation, *J. Geophys. Res.*, *90*, 543–547, doi:10.1029/JA090iA01p00543.

Vasyliunas, V. M. (1970), Mathematical models of magnetospheric convection and its coupling to the ionosphere, in *Particles and Field in the Magnetosphere, Astrophysics and Space Science Library,* vol. 17, edited by B. M. McCormack, and A. Renzini, pp. 60–71, Reidel Publishing, Dordrecht, The Netherlands.

Waters, C. L., B. J. Anderson, and K. Liou (2001), Estimation of global field aligned currents using the Iridium® system magnetometer data, *Geophys. Res. Lett.*, *28*, 2165–2168, doi:10.1029/2000GL012725.

Yang, J., F. R. Toffoletto, R. A. Wolf, S. Sazykin, P. A. Ontiveros, and J. M. Weygand (2012), Large-scale current systems and ground magnetic disturbance during deep substorm injections, *J. Geophys. Res.*, *117*, A04223, doi:10.1029/2011JA017415.

Zaharia, S., and C. Z. Cheng (2003), Near-Earth thin current sheets and Birkeland currents during substorm growth phase, *Geophys. Res. Lett.*, *30*, 1883, doi:10.1029/2003GL017456.